



## A universal fluoruous technology toward superhydrophobic coatings

Jinlong Zha, Nicolas Batisse, Daniel Claves, Marc Dubois

### ► To cite this version:

Jinlong Zha, Nicolas Batisse, Daniel Claves, Marc Dubois. A universal fluoruous technology toward superhydrophobic coatings. *Journal of Colloid and Interface Science*, 2019, 553, pp.778-787. 10.1016/j.jcis.2019.06.067 . hal-04051451

**HAL Id: hal-04051451**

**<https://uca.hal.science/hal-04051451>**

Submitted on 30 May 2023

**HAL** is a multi-disciplinary open access archive for the deposit and dissemination of scientific research documents, whether they are published or not. The documents may come from teaching and research institutions in France or abroad, or from public or private research centers.

L'archive ouverte pluridisciplinaire **HAL**, est destinée au dépôt et à la diffusion de documents scientifiques de niveau recherche, publiés ou non, émanant des établissements d'enseignement et de recherche français ou étrangers, des laboratoires publics ou privés.



Distributed under a Creative Commons Attribution - NonCommercial - NoDerivatives 4.0  
International License

# A universal fluororous technology toward superhydrophobic coatings

*Jinlong Zha<sup>1</sup>, Nicolas Batisse, Daniel Claves\*, Marc Dubois*

Université Clermont Auvergne, CNRS UMR 6296, Sigma Clermont, ICCF, F-63000  
Clermont-Ferrand, France

**Corresponding author:** daniel.claves@uca.fr (phone: +33 473 405 165 / fax: 407 108) –  
ICCF, Bât. Chimie 5, 24 Av. Blaise Pascal - TSA 60026, 63178 Aubière Cedex, France

**Co-authors:** nicolas.batisse@uca.fr / marc.dubois@uca.fr / zhajl@buaa.edu.cn

## Abstract

### *Hypothesis*

Development of a process yielding large-sized non-wettable coatings of immediate applicative interest seems feasible by associating a membrane spinning technique with the artificial mimic of a bio-inspired strategy toward water repellency. Accordingly, the question that arises is how to design a multiscale textured and chemically-activated continuous film.

### *Experiments*

A novel synergic combination of a processing technique and chemical treatment was developed in this purpose. Fluorinated nanocarbons were included in polyvinylpyrrolidone (PVP) microfibers *via* their addition in a precursor solution for electrospinning. The nanocomposites thus obtained were subsequently treated under gaseous molecular fluorine in mild conditions.

### *Findings*

Owing to the reactivity of PVP with F<sub>2</sub>, both etching and functionalization occurred during such a post-treatment. The chemical modification undergone by PVP upon fluorination has

---

<sup>1</sup> Present address : Key Laboratory of Bio-inspired Smart Interfacial Science and Technology, School of Chemistry, Beihang University, Beijing, 100191, China

been analyzed and a mechanistic approach proposed. An impressive dual texturing developed at the micro- and nanoscale thanks to the combined action of electrospinning, polymer etching and emergence of the nanofillers. This allowed a stable with time superhydrophobic coating-like film to be achieved.

**Keywords:** Electrospinning, Fluorine, Superhydrophobicity

**Declarations of interest:** none

## 1. Introduction

With a view to developing superhydrophobic surfaces, Nature can be a genuine source of inspiration. Stunning achievements in the matter are the leaves of several plants such as *Nelumbo nucifera* (Lotus), *Brassica oleracea* (cabbage), *Colocasia esculenta* (taro), the wings of butterflies,<sup>[1]</sup> legs of water striders<sup>[2]</sup> or feathers of some birds. A complex topography with multiple scales of roughness has often proven to be quite effective in generating high contact angles with water.<sup>[3]</sup> Hence, a surface with two levels of roughness can be considerably hydrophobic, even when each texture, considered separately, has only a small effect on water repellency.<sup>[4]</sup>

Herein, we have developed an innovative scheme toward highly hydrophobic surfaces, based on a combination of surface chemistry and the former bio-inspired multiscale argumentation. Hence, a primary texture could be obtained at a micrometric scale *via* electrospinning. This process appears as a powerful, simple and practical one-step method to generate continuous ultrathin fibers with micro-to sub-micrometer diameters from a wide variety of polymeric materials. In parallel, the introduction of hydrophobic chemical groups has been considered. Fluorine is known to induce a water-repellent effect<sup>[5]</sup> but most fluoropolymers are insoluble and therefore do not appear compatible with the electrospinning process. We have then turned to the incorporation of fluorine-containing compounds into a soluble polymer. To date, the use of fluorinated fillers in combination with electrospinning has not been extensively developed, in spite of significant potential benefits, like: i) stable dispersion in solvents commonly used for electrospinning ii) such fillers can act both as a source of fluorine and as reinforcing agents of electrospun fibers iii) when fillers emerge from electrospun fibers, some additional roughness might be created. At last, and in an ultimate step toward enhanced hydrophobicity, a post-fluorination concept was implemented, in order to access multiscale texturing through etching whilst increasing the final fluorine content.

The present approach is global in scope. It is only as a hands-on demonstration that it remains here focused on the use of polyvinylpyrrolidone (PVP) throughout all steps of the above-described process. Indeed, PVP is soluble in water and most of polar solvents. In solution, it exhibits excellent wetting properties and readily forms films. This makes it an excellent coating agent or coatings additive, especially for electrospinning. Fluorinated nanocarbons were here used as fillers, owing to their chemical inertness and nanometer size likely to induce the different scales ratio searched for. Thus, nanocomposites made of PVP microfibers filled with fluorinated carbonaceous nanomaterials of spherical (0 D) and cylindrical (1 D) shape, respectively, were successfully fabricated. Post-fluorination with F<sub>2</sub> gas was then performed in order to convert the initially hydrophilic nanocomposite films into superhydrophobic coatings, displaying spectacular multiscale inner architectures.

## 2. Experimental section

Content of the forthcoming sub-sections is described in fine details in Supporting Information document **SI1**.

### 2.1. Materials:

In brief, PVP was a commercial standard and graphitized carbon blacks<sup>[25]</sup> (GCBs) or carbon nanofibers (CNFs) were used as fillers precursors. These latter were directly fluorinated using pure fluorine gas for 3 h at 440 and 465 °C, respectively. Details on the synthesis conditions and fluorination mechanism are well described in previous work.<sup>[9]</sup> Swelling is noticed following fluorination owing to the F atoms accommodation. The fluorination level 'x' in CF<sub>x</sub> (i.e. F/C molar ratio) of our fluorinated GCBs and CNFs, determined by both weight uptake and quantitative NMR, are equal to 0.92 and 0.80, respectively. The corresponding samples, used as fillers, are denoted **FGCBs** and **FCNFs**.

## 2.2. Methods

*Electrospinning:* PVP solutions in ethanol, loaded with 22 w.% of the former fillers, were employed to fabricate fibers using the electrospinning method. For comparison, electrospun composite fibers with a non-fluorinated filler (CNFs or GCBs) were also prepared, from the same route. The non-woven mats thus obtained consisted of composite fibers and were preserved carefully in a moisture-free desiccator.

*Fluorination of electrospun fibers:* Cut pieces (1 cm<sup>2</sup>) of electrospun membranes were reacted at room temperature with an excess of pure fluorine gas at a controlled pressure, defining the amount of gaseous reagent involved in the reaction.

## 2.3. Characterizations

IR, XPS and NMR spectroscopies offered here an optimized analytical strategy. Indeed, XPS allows to quantitatively probing surface modifications over an unlimited range of elements, while its relative lack of resolution can be balanced using NMR for some more specific nuclei at the surface level, through cross-polarization experiments.

To measure the polar and dispersion components as well as the total surface energy, static contact angle measurements were carried out from the conventional Owens-Wendt method,<sup>[15]</sup> using two different liquids, namely distilled water and formamide.

## 3. Results and discussion

### 3.1. The pristine nanocomposites

After a fine and cumbersome tuning of experimental conditions, regular electrospun fibrous composites could be successfully prepared. The latter were then subsequently treated by molecular fluorine at room temperature. All related details are given in the former experimental section and document **SI1**. The following **Table 1** summarizes the post-fluorination conditions of our electrospun nanocomposites and the corresponding names used for each sample throughout the text.

**Table 1.** Fluorination conditions and notations.

Type	Filler	Notation	Electrospinning duration (min)	F <sub>2</sub>	Fluorination
				pressure (mbar)	duration (min)
PVP	None	PVP-F50	20	50	30
		PVP-F20-1	1	20	30
		PVP-F20-4	4	20	30
PVP/FGCBs	Fluorinated CF <sub>0.92</sub> 22 w.% Carbon black	PVP/FGCBs- F20-30min	20	20	30
		PVP/FGCBs- F50-30min	20	50	30
		PVP/FGCBs- F50-5min	20	50	5
		PVP/FCNFs- F20-30min	20	20	30
		PVP/FCNFs- F50-30min	20	50	30
PVP/FCNFs	Fluorinated Nanofibers	PVP/FCNFs- F50-5min	20	50	5

SEM images (**Figure 1**) evidence the efficiency of the selected electrospinning conditions in the preparation of uniformly shaped fibers, monodisperse in diameter (around  $1.5 \pm 0.2 \mu\text{m}$ ). No end can be observed and the entangled fibers appear smooth at their surface. When spherical fluorinated GCBs (50 nm average diameter) are incorporated at 22 w.%, the resulting electrospun composite fibers exhibit similar shape and diameter when compared to pure PVP. Higher magnification points out some surface roughness, however, with asperities having nearly the size of the nanofiller (**Figure 1d and e**). Lower relative contents of fillers (**Figure SI2e**) result in a decrease of the surface density of those asperities, which are then assigned to some emerging fluorinated filler particles. When fibrous fluorinated fillers with larger diameter (180 nm) and length (several microns) are used, the latter are clearly more apparent at the surface level in SEM images (**Figure 1f and g**). All filler nanofibers are trapped into the PVP matrix, some emerging and resulting in somewhat radial barbs, though most are oriented parallel to the PVP microfiber axis. Because of the high diameter of the nanofiller in this case, the composite microfibers slightly swell and their diameter can reach  $2 \mu\text{m}$  and more. Whatever the fillers relative content (from 7 to 22 w.%), no significant morphological difference could be observed following the use of raw fillers (GCBs or CNFs) or of their fluorinated counterparts (FGCBs or FCNFs). To illustrate this point, additional SEM images are shown in supplementary information (**Figure SI2**). The presence of fluorine atoms has then a negligible effect on the filler/matrix interface.

Multinuclear solid state NMR measurements were performed on the PVP/FCNFs nanocomposite so as to focus either on the PVP matrix ( $^1\text{H} \rightarrow ^{13}\text{C}$  CP-MAS experiment) or on the fluorinated filler ( $^{19}\text{F}$  MAS). The corresponding data are typical of non-interacting compounds in a mixture. The  $^1\text{H} \rightarrow ^{13}\text{C}$  CP-MAS spectrum (**Figure SI3a**) shows five types of carbons, unshifted in regard to pure PVP. The main line at -190 ppm in the  $^{19}\text{F}$  spectrum (**Figure SI3b**) is assigned to covalent C–F bonds as in conventional  $(\text{C}_2\text{F})_n$  and  $(\text{CF})_n$  graphite

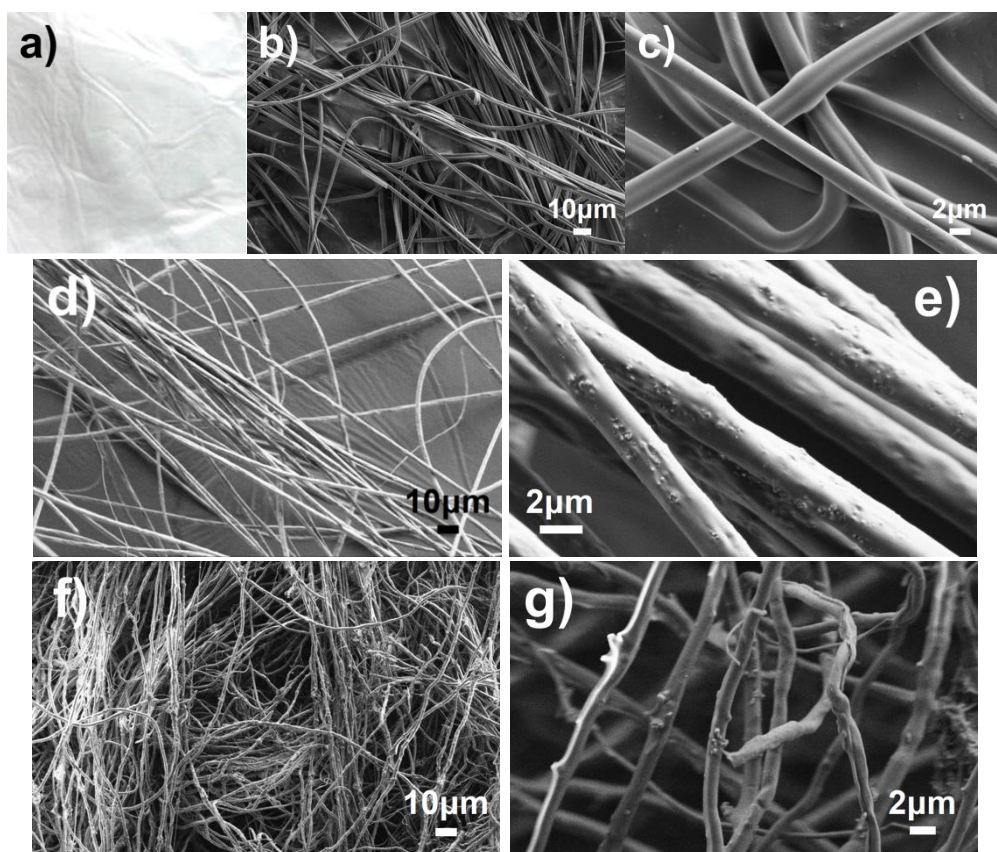


**Figure 1.** (a) Picture of a PVP electrospun membrane. (b-g) SEM images of electrospun fibers obtained from: (b, c) PVP, (d, e) PVP/FGCBs and (f, g) PVP/FCNFs.

fluorides. A few  $\text{CF}_2$  groups are also evidenced by a line at -120 ppm.<sup>[6]</sup> This spectrum is kept unchanged in comparison with that from “free” FCNFs. This unambiguously shows that no fluorine atom is transferred from the fluorinated filler to the PVP matrix. The same conclusion can be drawn for FGCBs.

Transmission infrared spectroscopy provides further support on this aspect, spectra consisting of the superimposition of the vibration bands of PVP with those of the fluorinated fillers (**Figure SI3**). All the characteristic vibrational bands of pure PVP are observed in accordance with the literature.<sup>[7]</sup> Thus, the similarity with the reported spectra of pure PVP again underlines that the polymer and fillers behave as independent phases.

### 3.2. Chemical transformation by post-fluorination

Pursuing our aim to prepare superhydrophobic films, the PVP surface had to be chemically modified in a second step, through introduction of hydrophobic functions. In this purpose, direct fluorination was carried out in mild conditions, in order to limit decomposition of the polymer under  $\text{F}_2$  gas ( $\text{CF}_4$  and  $\text{C}_2\text{F}_6$  gases evolved). For instance, decomposition is well known to compete with the covalent grafting of fluorine atoms by substitution at C-H sites in vinyl-based polymers.<sup>[8]</sup> Room temperature and low  $\text{F}_2$  pressures (20 and 50 mbar) were then used in addition to durations lower than or equal to 30 min (**Table 1**). Another way to mitigate the polymer reactivity consists in increasing the electrospun membrane thickness for a given  $\text{F}_2$  pressure. This could be easily done by varying the electrospinning duration from 1 to 4 min, respectively. It is to note that being saturated with fluorine on their surface,<sup>[9]</sup> nanofillers do not react with  $\text{F}_2$  at this temperature.

The chemical transformation undergone by the polymer matrix following the post-fluorination treatment has been analyzed separately, from pure PVP microfibers (no filler), through a cross combination of techniques (IR, XPS, RMN). In parallel to the polymer matrix chemistry, the effect of fluorination on the morphology of our electrospun fibers has been

studied using SEM. Indeed, the high reactivity of gaseous fluorine makes it an aggressive reagent, able to result in strong etching as a consequence of surface localized decomposition.<sup>[8]</sup> The following SEM images (**Figure 2**) show that the relatively mild conditions used here keep the overall morphology of fibers essentially unchanged, though the latter do not look as smooth as they do initially. No significant change in diameter can be established by careful examination of numerous SEM images. Therefore, adding to the chemical modification of the PVP surface, reasonable etching also occurs and a slight roughness progressively develops upon fluorination.

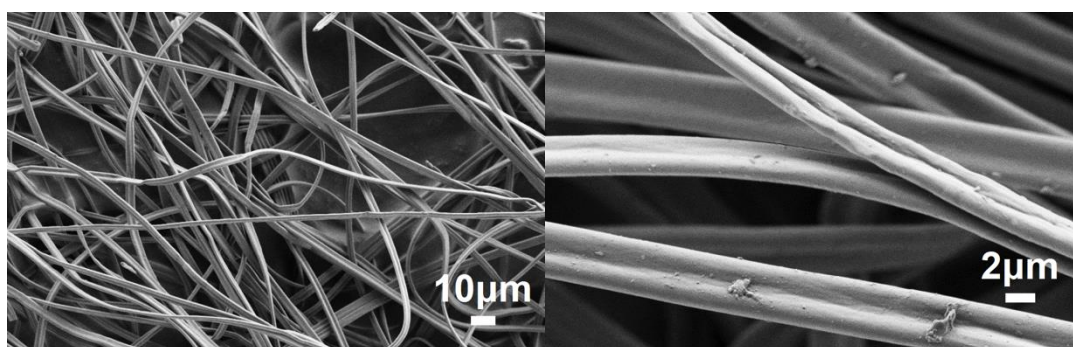


**Figure 2.** SEM images of the PVP-F50 sample.

In order to evidence the formation of covalent C-F bonds, NMR was carried out with different nuclei.  $^{19}\text{F}$  resonance (**Figure SI4a**) allowed us to probe the surface fluorinated layer formed. Typical bands<sup>[10]</sup> from CHF and  $\text{CF}_2$  groups can be evidenced, whose broadness stems from non uniform, more or less fluorinated chemical environments (e.g. for CHF groups:  $\text{CH}_2\text{-CHF-CH}_2$ ,  $\text{CHF-CHF-CHF}$ ,  $\text{CF}_2\text{-CHF-CHF}$ ,  $\text{CF}_2\text{-CHF-CF}_2$ ). A low intensity resonance assigned to  $\text{CF}_3$  moieties evidences their formation during fluorination. Such groups result from C-C bond cleavage in the polymer chain and/or ring, followed by perfluorination, and are good indicators of a partial decomposition during the reaction. The

presence of CHF, CF<sub>2</sub> and CF<sub>3</sub> is further confirmed by <sup>19</sup>F→<sup>13</sup>C CP MAS experiments (**Figure SI4b**). Cross-polarization also reveals CH<sub>2</sub>, C-N, N-C=O, N-COO, O=C-O-R and C=O groups, underlining that fluorine atoms are close enough to interact with those carbon atoms during CP experiments. <sup>1</sup>H→<sup>13</sup>C CP MAS measurements were also performed, giving information mainly about the bulk. The spectrum of the F50 sample, shown here as an example (**Figure SI4c**), is nearly similar to that of pristine PVP. However, <sup>1</sup>H nuclei also polarize F in CHF and CF<sub>2</sub> groups, resulting in corresponding minor bands and again, PVP happens unambiguously fluorinated.

Following fluorination, IR spectroscopy clearly shows a drastic splitting at the level of the absorption band arising from the initial C=O moiety in pristine PVP (**Figure SI4d**). Thus, an additional component emerging at 1735 cm<sup>-1</sup> seems to bear witness for the appearance of the ester function. At first glance, it might be surprising to generate some oxygenated groups from a fluorination reaction, but direct addition of molecular fluorine to polymers is well known to produce radical terminations prone to react with oxygen or atmospheric water upon air re-exposure.<sup>[8]</sup> The second essential characteristic in the IR spectra is a weak signal near 1250 cm<sup>-1</sup>, typical of C-F bonds. Though the latter moiety usually gives a strong absorption band, the small amplitude observed here has to be related to a reaction restricted to the outer surface of the fibers only. The intensity of the C-F band varies according to the fluorinated PVP sample and qualitatively, with an increasing fluorine ratio: F20-4 < F20-1 << F50 (changing the electrospinning duration from 1 to 4 min, results in a thicker membrane and therefore in a lower F:PVP mass ratio for a given F<sub>2</sub> pressure).

The C<sub>1s</sub>, N<sub>1s</sub>, O<sub>1s</sub> and F<sub>1s</sub> XPS spectra obtained from three different samples of fluorinated PVP microfibers are displayed in **Figure SI5**. Evolution in the surface composition upon fluorination, established from the elements area ratios taking into account relative sensitivity factors, is summarized in **Table 2** and is here written relative to the 6 C

**Table 2.** Surface nominal and functional compositions of the initial and fluorinated PVP membranes.

<b>Sample +</b>	
<b>Surface composition</b>	<b>Functional composition (relative to 1 C)</b>
<b>Raw PVP</b>	
$-(C_6H_9NO)_n -$	$C_{0,5}(CN)_{0,33}(NCO)_{0,17}$
<b>PVP-F20-1</b>	
$-(C_6H_{4,3}N_{0,8}O_{1,7}F_{4,7})_n -$	$C_{0,17}(CN/C-O)_{0,22}(CHF/C=O)_{0,30}(NCOO)_{0,16}(CF_2)_{0,13}(CF_3)_{0,02}$
<b>PVP-F20-4</b>	
$-(C_6H_{4,7}N_{0,6}O_{1,3}F_{4,3})_n -$	$C_{0,32}(CN/C-O)_{0,16}(CHF/C=O)_{0,23}(NCOO)_{0,15}(CF_2)_{0,11}(CF_3)_{0,02}$
<b>PVP-F50</b>	
$-(C_6H_{3,5}N_{0,7}O_{1,3}F_{5,5})_n -$	$C_{0,13}(CN/C-O)_{0,19}(CHF/C=O)_{0,22}(NCOO)_{0,19}(CF_2)_{0,24}(CF_3)_{0,04}$

atoms present in the initial monomer. The most salient features consist of an effective fluorine addition to the polymer matrix and a notable increase in the oxygen content, confirming former observation with the help of IR spectroscopy of the emergence of oxygenated functions. A decrease in the nitrogen content bears witness for partial degradation of the polymer. No strict correlation between the final amount of added fluorine and the levels of oxygen addition or nitrogen depletion can be established, however. Deconvolutions take account of potential contributions from some residual unreacted PVP. This happens possible provided care is taken to introduce drastic constraints, preliminary established from pure PVP as a blank, in profile, relative intensities and positions, over the related components. Hence, the persistence of weak related signals highly likely shows that the entangled fibers hinder gaseous fluorine from reaching some discrete parts of the samples and that a homogeneous surface halogenation cannot be achieved at the timescale of the experiments.

The basis of the structural analysis performed here is detailed in the case of the PVP-F20-1 sample only, the scheme being repeated from sample to sample. Hence, in comparison with PVP, a dramatic shift in the  $O_{1s}$  envelope toward higher core energies occurs, showing full chemical transformation of the lactam ( $N-C=O$ ) functional group of the cyclic monomer upon fluorination. The  $O_{1s}$  spectrum has been initially split into two contributions clearly appearing through a well-developed shoulder at high energies. With reference to standard tables, the corresponding chemical shift values suit quite well to the C-O and C=O moieties of a carboxylic group, again in agreement with the results of IR spectroscopy. Both signals being of equal magnitude in such a case, addition of a third contribution happened therefore necessary considering the obvious intensity difference exhibited by the spectrum. Thus, the final fit includes twin photoelectron peaks constrained with the same intensities and an additional contribution overlapping with that stemming from the C=O moiety of the former O-C=O function. This clearly points out the presence of pure carbonyl groups in the final product as well. The respective ratio of the carboxylic and carbonyl compounds is subject to change from sample to sample and independent of the final amount of added fluorine.

The  $N_{1s}$  spectrum appears significantly upshifted and could be well fitted with the help of two contributions only. The position in energy of the major photoemission signal suits very well to the carbamate ( $N-COO$ ) group, suggesting bridging of the formerly established carboxylic group with the remaining N atom from the initial cycle. It is well known that any acidic form is highly unstable in standard conditions, contrarily to esterified forms, so that the creation of a carbamic acid ester is highly likely to have occurred. A smaller amplitude feature at high binding energies indicates some additional N atoms in an electronegative environment. Tables of chemical shifts are much less documented for the latter element and a formal assignment has not been attempted, though the scarce possibilities seem here limited to N-O, N-F or still N-CF<sub>x</sub>, fluorine being the lone element able to induce a secondary shift. Thus, the corresponding group will be denoted N-X.

A correct deconvolution of the C<sub>1s</sub> clump is obtained through a set of six reasonably well resolved peaks with at least 0.8 eV separation. From standard tables and literature dedicated to fluorinated polymers,<sup>[11]</sup> the characteristics of >CHF and >CF<sub>2</sub> groups can be clearly identified. A low amount of –CF<sub>3</sub> terminations seems to be detected as well. The signature of the previously identified N-COO function clearly emerges, in parallel with that of the C-N junction as in PVP. Such an assignment yields the functional compositions listed in **Table 2** for the different samples. Not surprisingly, it can be easily observed that a progressive increase in the overall fluorine content coincides fairly well with a depletion of residual CH<sub>2</sub> groups and with a parallel increase of CHF groups, the latter being finally replaced by CF<sub>2</sub> upon further fluorine addition. It is then highly likely that H gets substituted by F and that the final hydrogen content in the formula (see **Table 2**) can be confidently assessed through the difference between the number of H atoms in the initial monomer formula and the number of F in its fluorinated counterpart. All F<sub>1s</sub> spectra (**Figure SI5**) have the shape of an apparently single peak at a rather usual binding energy<sup>[11]</sup> of  $688,0 \pm 0,2$  eV, with no possibility to separate respective contributions inherent to CF<sub>2</sub> or CHF. Assignments of all XPS signal are summarized in **Table SI6**.

Therefore, at this stage, the O<sub>1s</sub> and N<sub>1s</sub> spectra analysis allows two different reaction schemes to be inferred, as described in **Figure 3**. The slight decrease observed in the overall N content following fluorination indeed provides clue in favor of the structural alteration proposed in **Figure 3**, at the level of the initial heterocycle. Partial elimination of N through direct fluorination of an amidic polymer has already been reported<sup>[12]</sup> and also further supports these provisional schemes. The persistence of the C-N junction in the C<sub>1s</sub> spectrum might indicate that fluorination induces no modification either on the left side of the heterocycle or at the lower level alkyl branching, in agreement with the structures proposed here. A signal stemming from the C-O-C moiety of the carbamic acid ester might interfere in this region of the spectrum, however. The parallel reaction schemes inferred here also gain

credence from somewhat realistic mechanistic considerations. As a matter of fact, the competition envisaged seems to be easily justified through the most classical radical substitution or addition to a double bond mechanistic approaches. Hence, it is well known that direct substitution of H atoms of an alkyl chain with halogens is initiated by radical species. The propagation step is usually written  $R-H + X\cdot \rightarrow R\cdot + HX$  and  $R\cdot + X_2 \rightarrow R-X + X\cdot \dots$  etc. Such a mechanism is here highly favored by the easy homolytic bond cleavage of the  $F_2$  molecule at room temperature, due to its weak bond energy. It is then interesting to note, in favor of the reaction schemes proposed, a seemingly nice opportunity for the preferential formation of a potentially stable intermediate radical species in the alpha-position of the carbonyl function (**Figure 3**), with great potency to direct chemical balance toward a carboxylic final product upon air re-exposure. As shown in the figure, its cyclic nature makes it a secondary carbon radical species, therefore exhibiting relatively good stability, enhanced here *via* resonance with the lone pairs of electrons on the adjacent oxygen atom of the carbonyl group. The formation of such a plausible reaction intermediate might not be necessarily spontaneous but might also stem from successive rearrangements within a first radical.

In parallel, it is common knowledge that the bond located between nitrogen and the C=O moiety along the amide functionality is extremely reactive and the main cleavage site of this function. It can be confidently claimed that, owing to the lone-pair donor effect of N, such an electron-rich site is privileged regarding an attack by quite an electrophilic species as fluorine. Such a mechanism could therefore well explain the occurrence of N in an electronegative environment following fluorination, and direct chemical balance toward a carbonyl compound, in compliance with the second scheme proposed here.

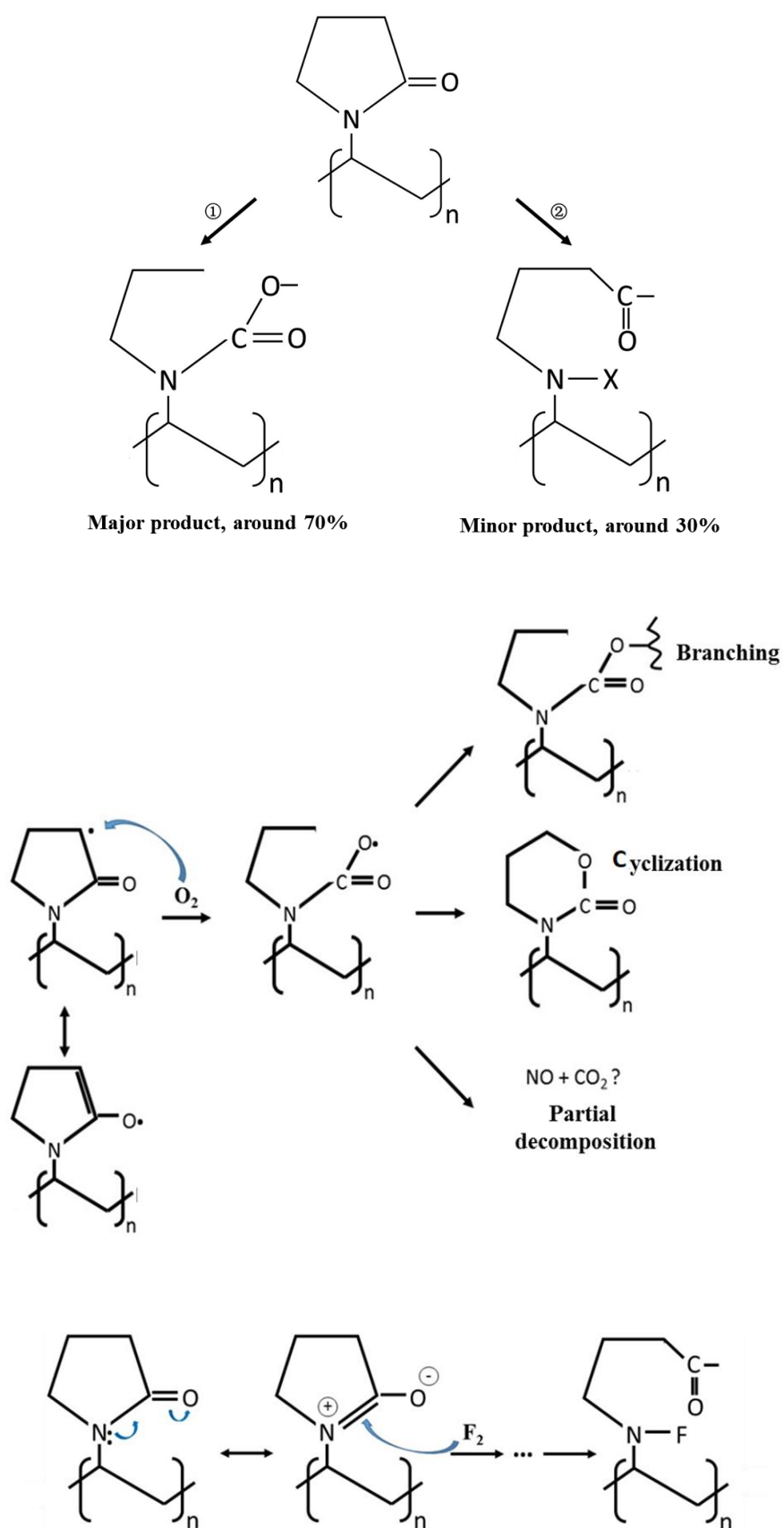


**Figure 3.** Reaction schemes occurring upon fluorination of PVP and plausible main steps of a mechanistic approach of fluorine addition to PVP followed by re-exposure to air.

### 3.3. Polymer matrix fluorination and wettability

Whereas pristine PVP films are water-soluble, water contact angles of  $140\pm4^\circ$ ,  $142\pm3^\circ$  and  $129\pm4^\circ$  arose for the F20-1, F20-4 and F50 samples, respectively (**Table 3**). This strong hydrophobicity obviously partly arises from the surface chemical modification previously performed. Indeed, the surface energy of a material depends on the character of terminal groups and substitution of the hydrogen atoms of hydrocarbons by fluorine tends to make it decrease, because of the strong covalence and small polarizability of the C-F bond. The surface tension of a solid surface is proportional to the surface fluorine atomic ratio<sup>[5]</sup> and decreases in the order  $-\text{CH}_2 \rightarrow -\text{CHF} \rightarrow -\text{CF}_2 \rightarrow -\text{CF}_3$ , up to a critical value of 67 dyn/cm for the later termination. Nevertheless, the presence of fluorinated groups on the fibers surface and the subsequent surface energy decrease cannot be sufficient to reach superhydrophobicity, since flat surfaces with  $-\text{CF}_3$  terminal groups exhibit a maximum contact angle of  $120^\circ$  only<sup>[5]</sup> and adding nano- or micro-texturing is necessary in this purpose. This additional role played by even a small difference in texture is well exemplified here since the F50 sample, with the highest fluorination rate, yet exhibits the lowest contact angle.

The Wenzel and Cassie-Baxter models can be used to understand the influence of surface roughness. When water droplets on a micro-textured surface are in the Wenzel state,<sup>[13]</sup> the whole surface roughness is completely wetted. The Wenzel equation is  $\cos \theta_c = r \cdot \cos \theta_c^Y$ , where  $r$  is a roughness parameter. The results obtained here cannot be explained from the Wenzel equation because it is possible to obtain extremely high  $\theta_c$  only if  $\theta_c^Y > 90^\circ$ . Only the Cassie-Baxter equation can predict extremely high  $\theta_c$  regardless of the  $\theta_c^Y$  value, which indicates the presence of air between the droplet and the surface.<sup>[14]</sup> The Cassie-Baxter equation is  $\cos \theta_c = r_f \cdot f \cdot \cos \theta_c^Y + f - 1$ , where  $r_f$  is the roughness ratio of the substrate wetted by the liquid,  $f$  the solid fraction and  $(1 - f)$  the air fraction. This equation can lead to

**Table 3.** Water contact angles of fluorinated PVP and composites films.

Raw PVP		Fluorinated PVP		
Soluble		F20-1	F20-4	F50
		140±4°	142±3°	129±4°
Fluorinated PVP/CNFs 22%		Fluorinated PVP/FCNFs		
F20-30 min	F50-30 min	F20-30 min	F50-5 min	F50-30 min
130±3°	133±4°	151±5°	153±5°	152±5°
Fluorinated PVP/FCGBs				
		F20-30 min	F50-5 min	F50-30 min
		143±4°	135±6°	142±7°

superhydrophobic properties if the air fraction is extremely important or to highly hydrophobic properties if the air fraction is less important.

So far, our fluorinated PVP membranes are “only” highly hydrophobic because their surfaces are micro-textured but not nano-textured. Therefore, in the following and in order to further enhance hydrophobicity, we will exploit the potency arising from the presence of fluorinated fillers to change the roughness. It is expected that the latter can provide some additional nano-texturing which will exacerbate the Cassie-Baxter state.

### 3.4. Multiscale morphological transformation by post fluorination

Composites including 22 w.% of FCNFs or FGCBs fillers were then treated under fluorine in the same conditions than PVP fibers (20 and 50 mbar - see **Table 1**). The duration for 50 mbar was even reduced to 5 min so as to also test milder reactive conditions. SEM images clearly evidence development of the additional nano-texturing expected, which appears interestingly complex, as shown in **Figure 4** and **5** (for comparison, the effect of the

same post-fluorination treatment on a composite made from a non-fluorinated filler is displayed in **figure SI7**). Etching (due to partial decomposition) of PVP occurred, inducing a spectacular new multiscale texture. This is particularly well highlighted in the PVP/FGCBs case (**Figure 4**). With a F<sub>2</sub> pressure of 50 mbar for 5 min, etching happens to be limited but microfibers are clearly cut to shorter lengths (**Figure 4a, b and c**), while their surface roughness is moderately increased owing to the short reaction time. More drastic conditions (20 mbar for 30 min - **Figure 4d, e and f**) result in the fragmentation of microfibers, though their initial cylindrical shape is preserved. Nano-texturing is clearly apparent in **figure 4f**. A similar trend in the etching degree was observed from the PVP/FCNFs composite, i.e. F50-5 min < F20-30 min < F50-30 min. The main difference seems to be the maintaining of the microfibers length (**Figure 5a and d**), at least for F50-5 min and F20-30 min. Though more frequent disruptions can be observed following application of the most severe conditions F50-30 min (**Figure 5g**), the thus treated fibers body remains long in comparison with the case of PVP/FGCBs fibers treated similarly.

Obviously, the texturing effect obtained arises from the surface limited partial decomposition of the polymer matrix upon reaction with fluorine gas. When a surface layer of organic component is thus etched away, those nanofillers initially located near the surface level show up. Interestingly, the fibrous imprint maintained following more or less severe attack by fluorine unravels the nanofillers dispersion through the bulk of the pristine electrospun fibers (**Figure 4 and 5**). Therefore, topographical differences between post-fluorinated FGCBs/FCNFs-based composites can be explained by taking into account FCNFs length (several microns) and their alignment with the axis of the electrospun microfiber. **Figure 6** depicts a sketchy scenario, in which fluorinated nanofibers prevent too frequent disruptions within the composite microfibers, while the short size and spherical shape inherent to the FGCBs filler results in more fragmentation, especially in drastic fluorination conditions (F20-30 min).

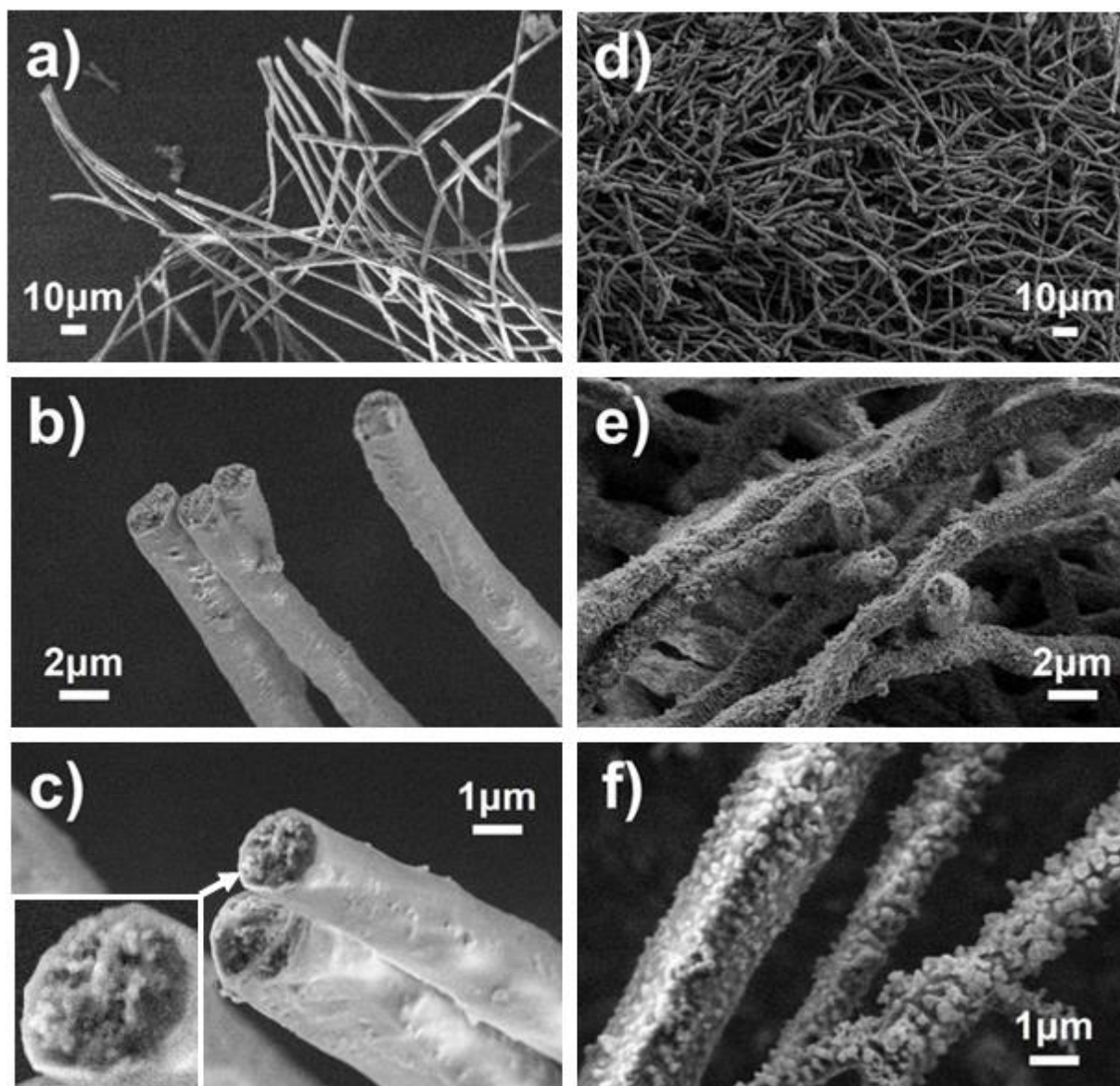


**Figure 4.** SEM images of fluorinated PVP/FGCBs composite fibers: (a, b, c) F50-5min and (d, e, f) F20-30min.

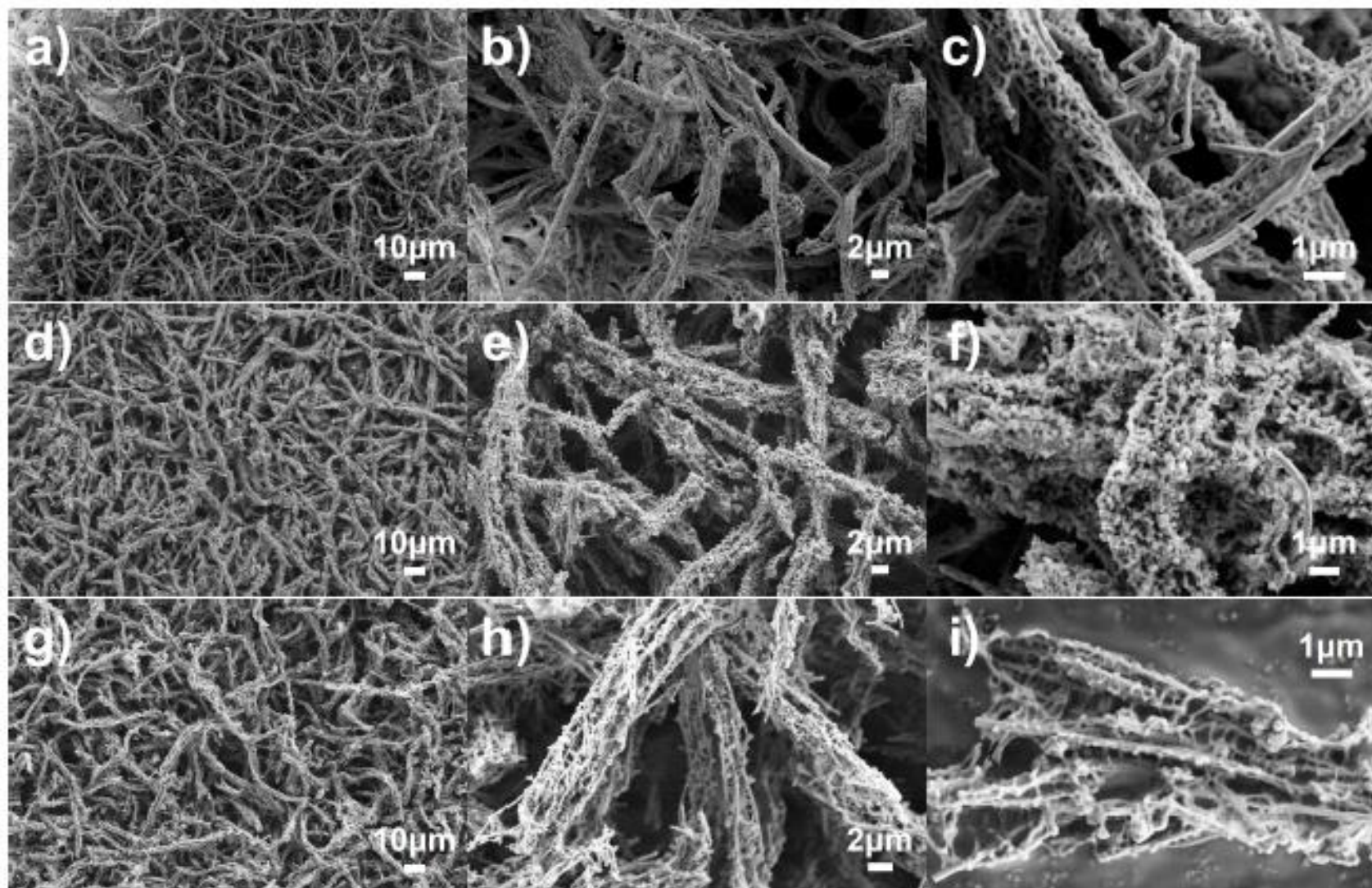


**Figure 5.** SEM images of fluorinated PVP/FCNFs composite fibers: (a, b, c) F50-5min, (d, e, f) F20-30 min and (g, h, i) F50-30min.

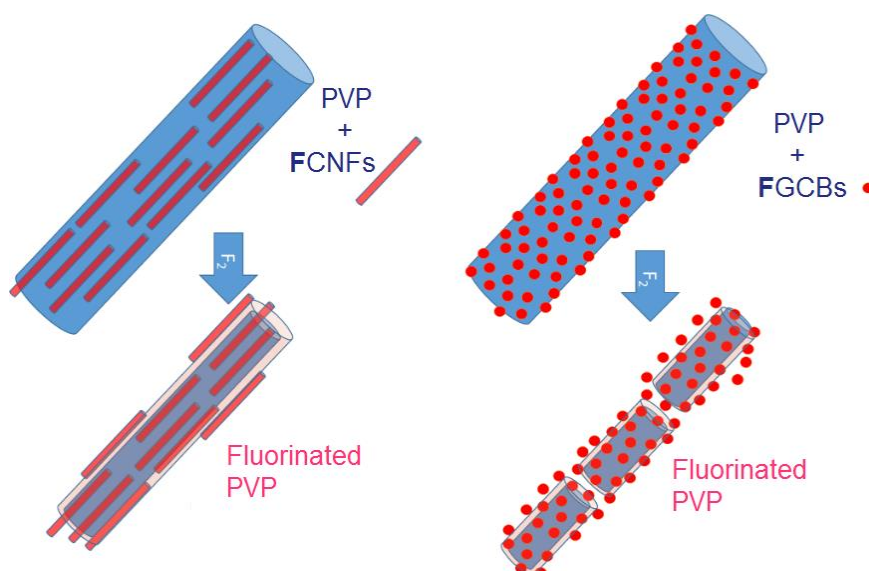


**Figure 6.** Schematic view of the post-fluorination effect on electrospun nanocomposite fibers.

Overall, etching our composites with fluorine results in an impressive effect and as initially expected, has proven extremely efficient in the development of a multiscale roughness.

### 3.5. Post-fluorinated composites and wettability

It is here important to note that all samples still present a woven-like film aspect following post-fluorination, whatever the conditions used, which allowed contact angle measurements to be performed. Superhydrophobicity turned out to be reached with PVP/FCNFs samples, whatever the fluorination conditions, with contact angles all exceeding  $150^\circ$  (**Table 3** and **Figure 7**). If non-fluorinated CNFs are used as fillers, contact angles are significantly lower (about  $130^\circ$ ) and the presence of fluorine atoms in the fillers seems therefore to be an important supplementary factor toward texturing and consequently, toward superhydrophobicity. Because of the seemingly optimal dual texturing obtained from the fluorinated PVP/FCNFs composite, i.e. micro- (via electrospinning) and nanosizing (nanofillers plus etching by fluorination), air is trapped in the cavities and the Cassie-Baxter

state is reached, allowing contact angles to exceed the threshold of  $150^\circ$ . A similar phenomenon occurs for PVP/FGCBs but fragmentation of the microfibers and the numerous asperities of about 50 nm created seem not efficient enough to raise the contact angle up to the critical value marking an entry into superhydrophobicity.

The total surface energy, polar and dispersive components, relating to the superhydrophobic samples were calculated using the conventional Owens-Wendt method<sup>[15]</sup> (**Figure 8**). The polar component is found to slightly increase with the formation of oxygenated groups (see discussion above). The decrease of the total energy is then mainly due to the drop of the dispersive part which is directly related to the additional nano-texturing created. A particular attention was devoted to the time dependence of the contact angles in the case of the fluorinated PVP and (F50-30 min) PVP/FCNFs samples (**Figure SI8**). Indeed, the partial fragmentation of microfibers during fluorination may result in fragile films. Moreover, if residual non-fluorinated PVP is still present, its solubility in water may induce changes in the superhydrophobic character through change in the fibers morphology. It turned out that for a fluorinated PVP electrospun membrane with no filler, the contact angle dropped to  $100^\circ$  in 7 min. On the contrary, an angle higher than  $150^\circ$  was maintained for at least 10 min with a fluorinated PVP/FCNFs composite. Such different behaviors can be easily explained from SEM observations (**Figure SI9a, b, c**) performed once such samples have been rinsed with plenty of water, on a trial basis. The micro-texturing is then seen to collapse in the case of fluorine-treated pure PVP fibers because of the solvation of the non-fluorinated inner part of the polymer matrix, while the overall morphology is maintained when fluorinated CNFs nanofillers are incorporated into the electrospun fibers (**Figure SI9c**), thus reinforcing them (the removal of the core yields hollow tubes and the 100-200 nm thickness of the fluorinated PVP layer can even be distinguished on image **SI9d**). Both micro- and nano-texturing scales

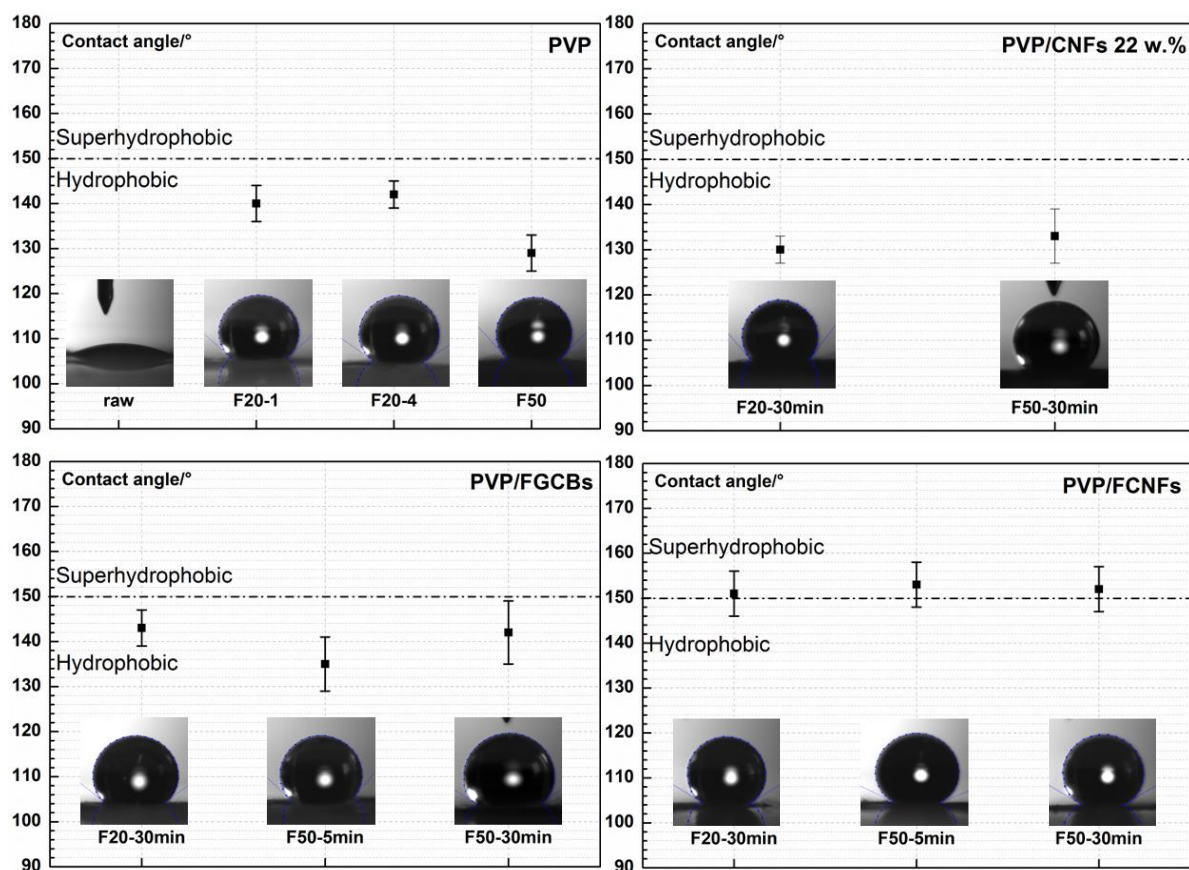


**Figure 7.** Contact angles of post-fluorinated PVP and composite membranes, respectively.

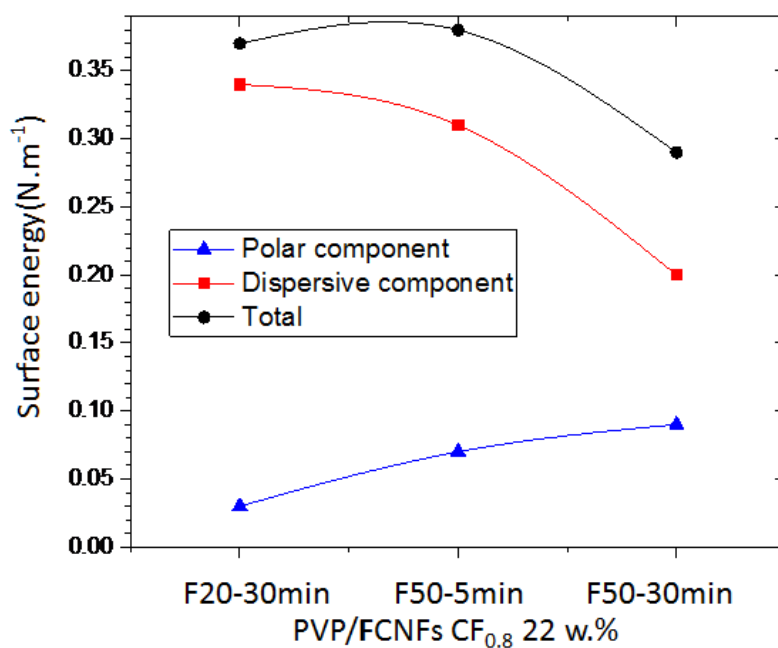


**Figure 8.** Changes upon post-fluorination in the dispersive and polar components and in the related total surface energy.

persist in this case, completing the chemically-induced hydrophobic character issuing from the presence of stable C-F bonds, and superhydrophobicity can then be maintained over a long time.

#### **4. Conclusion**

The need for solutions to a wide variety of problems spanning, but not limited to, tribologic issues (industrial pipelines, drag reduction in fluids into micro/nano channels ...) to anti-grip or even self-cleaning surfaces (windows, solar panels, roof tiles, anti-biofouling, textiles, plane de-icing ...), underlines the importance of technologies dedicated to superhydrophobic interfaces. The incorporation of properly selected nanofillers into electrospun microfibers combined with an adequate surface chemical treatment sheds light on how to design a large scale continuous film mimicing known hydrophobic bio-processes. It has thus been shown here that chemical activation by fluorinated groups, associated to a complementary multiscale texture arising from the electrospinning technique itself (microscale) plus chemical etching by molecular fluorine, which partly releases embedded nanoparticles (nanoscale), can lead to superhydrophobicity. The present work evidences that the technology developed is a highly promising route toward superhydrophobic films that may be used to cover almost any large-sized surface. Though PVP and fluorinated nanofibers offer here an excellent combination, the latter merely serve as a proof of concept. The multitude of polymers that can be processed by electrospinning as well as the diversity of fluorinated nanofillers that can be made available make this newly proposed strategy rugged, highly versatile and adaptable to many issues, given the efficiency of the electrospinning technique in coating objects with complex shapes.

The main trends emerging from a survey of the body of literature dedicated to fluorine-oriented methods bear witness for the innovativeness of the approach developed here as well as for its efficiency and relative simplicity. Indeed, the synergic “etching -

nanoparticles - electrospinning“ combination in order to directly induce characteristics leading to strong hydrophobicity, i.e. simultaneous functionalization and multiscale texturation, has not been reported previously. Furthermore, the use of molecular fluorine on an electrospun membrane has been extremely scarce to date. Hence, direct fluorination of electrospun poly(vinyl alcohol) fibers was reported,<sup>[16]</sup> leading to the introduction of CF<sub>2</sub> groups at high fluorine pressure, which made the surface of the fibers hydrophobic but resulted in their swelling as the only texturation effect obtained. It also turns out that post-fluorination of electrospun membranes has allowed us circumventing any difficulty related with the direct processing of fluoropolymers by electrospinning, as the latter are too insoluble and often exhibit too low dielectric constants. This happens to be the fundamental reasons why most former studies dealing with fluorine-containing electrospun membranes<sup>[17]</sup> have turned to complex routes involving pre-functionalization or copolymerisation with fluorinated sequences in the preparation of the precursor polymer, and our method further affords avoiding such steps. Additionnally, specific problems like an abnormal low surface fluorine content, sometimes detected<sup>[18]</sup> in the case of such electrospun fibers made from a soluble fluorinated segments-grafted polymer, can also be avoided as the presently proposed post-fluorination process ensures a uniform enrichment on the surface. Finally, the present work notably differs from most techniques reported to date which consist in covering fibers made from conventional soluble polymers with fluorinated compounds.<sup>[17,19-21]</sup> For instance, superhydrophobic/superoleophilic nanofibrous membranes made of cellulose acetate have been obtained thanks to a coating with a layer of SiO<sub>2</sub> nanoparticles previously functionalized with fluorinated polybenzoxazine.<sup>[19]</sup> Electrospinning was also previously associated to initiated chemical vapor deposition (iCVD) to coat poly(caprolactone) fibers with a thin layer of hydrophobic polymerized perfluoroalkyl ethyl methacrylate.<sup>[20]</sup> The graft polymerization of 3-trimethoxypropyl methylacrylate with poly(vinylidene fluoride) followed by electrospinning and subsequent fluorine coupling was also successfully tested.<sup>[21]</sup> Other

complex routes requiring the blending of different kinds of nanoparticles (PTFE,<sup>[22]</sup> TiO<sub>2</sub> and graphene<sup>[23]</sup>) or fluorinated ionic liquid (BMIPF<sub>6</sub>)<sup>[24]</sup> with a polymer solution before electrospinning were attempted to increase fibers surface roughness, but further work to stabilize the related hydrophobic properties must still be developed. On the contrary, our data evidence a stable superhydrophobic behavior.

Our new strategy is highly adaptable to impart to almost any large-sized surface a superhydrophobic character, as electrospinning can be extensively used for coating. It involves rather simple preparation, making it cost-effective, and offers clear advantages in comparison to strategies formerly developed. All of the aforementioned potentialities are highly desirable on an industrial scale.

**Supporting Information:** Documents, Figures and Tables SI1 to SI9 are available as supporting information.

## References

- [1] P. P. Goodwyn, Y. Maezono, N. Hosoda, K. Fujisaki, *Naturwissenschaften* 2009, 96, 781
- [2] X. Gao, L. Jiang, *Nature* 2004, 432, 36
- [3] N. J. Shirtcliffe, G. McHale, S. Atherton, M. I. Newton, *Adv. Colloid. Interface Sci.* 2010, 161, 124
- [4] N. J. Shirtcliffe, G. McHale, M. I. Newton, G. Chabrol, C. C. Perry, *Adv. Mater.* 2004, 16, 1929
- [5] a) Y. Chong, N. A. Watanabe, *J. Fluorine Chem.* 1991, 54, 43; b) T. Nishino, K. Nakamae, M. Matsushita, Y. Ueda, *Langmuir* 1999, 15, 4321
- [6] a) M. Dubois, J. Giraudet, K. Guérin, A. Hamwi, Z. Fawal, P. Pirotte, F. Masin, *J. Phys. Chem. B* 2006, 110, 11800; b) J. Giraudet, M. Dubois, K. Guérin, C. Delabarre, A. Hamwi, F. Masin, Solid-state NMR study of the post-fluorination of (C<sub>2.5</sub>F)<sub>n</sub> fluorine-GIC. *J. Phys. Chem. B* 2007, 111, 14143; c) T. Mallouk, B. L. Hawkins, M. P. Conrad, K. Zilm, G. E. Maciel, N. Bartlett, *Phil. Trans. Royal Soc. A: Math., Phys. and Eng. Sci.* 1985, 314, 179; d) A. Panich, *Synth. Met.* 1999, 100, 169
- [7] a) A. Slistan-Grijalva, R. Herrera-Urbina, J. F. Rivas-Silva, M. Ávalos-Borja, F. F. Castellón-Barraza, A. Posada-Amarillas, *Mater. Res. Bull.* 2008, 43, 90; b) T. Çaykara, S. Demirci; Ö. Kantoğlu, *Polym-plast. Technol.* 2007, 46, 737; c) A. F. Basha, *Polym. J.* 2010, 42, 728; d) L. S. Taylor, F. W. Langkilde; G. Zografi, *J. Pharm. Sci.* 2001, 90, 888; e) N. Tanaka, K. Ito, H. Kitano, *Macromol. Chem. & Phys.* 1994, 195, 3369
- [8] a) A. Kharitonov, *Prog. Org. Coat.* 2008, 61, 192; b) A. Kharitonov, R. Taege, G. Ferrier, V. V. Teplyakov, D. A. Syrtsova, G.-H. Koops, *J. Fluorine Chem.* 2005, 126, 251; c) A. P. Kharitonov, *J. Fluorine Chem.* 2000, 103, 123; d) A. P. Kharitonov, G. V. Simbirtseva, V. M. Bouznik, M. G. Chepezubov, M. Dubois, K. Guérin, A. Hamwi, H. Kharbache, F.

- Masin, J. Polym. Sci. Part A Polym. Chem. 2011, 49, 3559; e) A. Kharitonov, R. Taege, G. Ferrier, N. Piven, Surf. Coat. Int. Part B: Coat. Trans. 2005, 88, 201; f) P. Carstens, S. Marais, C. Thompson, J. Fluorine Chem. 2000, 104, 97 g) V. Nazarov, J. Appl. Polym. Sci. 2005, 95 (4), 897
- [9] F. Chamssedine, M. Dubois, K. Guérin, J. Giraudet, F. Masin, D. A. Ivanov, L. Vidal, R. Yazami, A. Hamwi, Chem. Mat. 2007, 19, 161
- [10] a) R. K. Harris, G. A. Monti, P. Holstein, Studies in Phys. and Theor. Chem. 1998, 84, 253; b) R. K. Harris, G. A. Monti, P. Holstein, Studies in Phys. and Theor. Chem. 1998, 84, 667; c) R. K. Harris, P. Jackson, Chem. Rev. 1991, 91, 1427
- [11] a) G. Beamson, D. Briggs, High Resolution XPS of Organic Polymers - The Scienta ESCA300 Database, Wiley Interscience, 1992; b) D. Claves, New J. Chem. 2011, 35 (11), 2477
- [12] A. Kharitonov, Y. L. Moskvina; D. Syrtsova, V. Starov, V. Teplyakov, J. Appl. Polym. Sci. 2004, 92 (1), 6
- [13] R. N. Wenzel, Indus. & Eng. Chem. 1936, 28, 988
- [14] A. Cassie, S. Baxter, Trans. Faraday Soc. 1944, 40, 546
- [15] D. K. Owens, R. Wendt, J. Appl. Polym. Sci. 1969, 13, 1741
- [16] J. S. Im, J. Yun, Y. M. Lim, H. I. Kim, Y. S. Lee, Acta Biomater. 2010, 6, 102
- [17] a) I. Sas, R. E. Gorga, J. A. Joines, K. A. Thoney, J. Polym. Sci. Part B: Polym. Phys. 2012, 50, 824; b) A. Singh, L. Steely, H. R. Allcock, Langmuir 2005, 21, 11604; c) S. Agarwal, S. Horst, M. Bognitzki, Macromol. Mater. Eng. 2006, 291, 592; d) M. Ma, R. M. Hill, J. L. Lowery, S. V. Fridrikh, G. C. Rutledge, Langmuir 2005, 21, 5549; e) L. Yi, X. Meng, X. Tian, W. Zhou, R. Chen, J. Phys. Chem. C 2014, 118, 26671; f) K. Acatay, E. Simsek, C. Ow-Yang, Y. Z. Menceloglu, Angew. Chem. Int. Ed. Engl. 2004, 43, 5210; g) L. Valtola, A. Koponen, M. Karesoja, S. Hietala, A. Laukkanen, H. Tenhu, P. Denfle, Polymer 2009, 50, 3103

- [18] W. Wu, G. Yuan, A. He, C. C. Han, *Langmuir* 2009, 25, 3178
- [19] Y. Shang, Y. Si, A. Raza, L. Yang, X. Mao, B. Ding, J. Yu, *Nanoscale* 2012, 4, 7847
- [20] M. Ma, Y. Mao, M. Gupta, K. K. Gleason, G. C. Rutledge, *Macromol.* 2005, 38, 9742
- [21] Y. Chen, H. Kim, *Appl. Surf. Sci.* 2009, 255, 7073
- [22] R. Menini, M. Farzaneh, *Polym. Int.* 2008, 57, 77
- [23] R. Asmatulu, M. Ceylan, N. Nuraje, *Langmuir* 2011, 27, 504
- [24] X. Lu, J. Zhou, Y. Zhao, Y. Qiu, J. Li, *Chem. Mat.* 2008, 20, 3420
- [25] a) A. Magasinski, P. Dixon, B. Hertzberg, A. Kvit, J. Ayala, G. Yushin, *Nature Materials* 2010, 9, 353; b) J. B. Donnet, R. C. Bansal, M. J. Wang, *Carbon black : science and technology*, Dekker, 1993